Japanese Journal of Applied Physics

REGULAR PAPER

Internal pressure dependence on viscoelasticity of arterial wall by ultrasonic measurement

Japanese Journal of Applied Physics **62**, SJ1041 (2023) **REGULAR PAPER**
https://doi.org/**10.35848/1347-4065/acbf5d**

Internal pressure dependence on viscoelasticity of arterial wall by ultrasonic measurement

Saki Suzuki[1], Shohei Mori[2], Masumi Iwai-Takano[1,3,4], Mototaka Arakawa[1,2*], and Hiroshi Kanai[1,2]

[1]*Graduate School of Biomedical Engineering, Tohoku University, Sendai, Miyagi 980-8579, Japan*
[2]*Graduate School of Engineering, Tohoku University, Sendai, Miyagi 980-8579, Japan*
[3]*Department of Epidemiology, Fukushima Medical University, Fukushima 960-1295, Japan*
[4]*Division of Cardiovascular Surgery, Fukushima Medical University, Fukushima 960-1295, Japan*

[*]E-mail: arakawa@tohoku.ac.jp

Received November 15, 2022; revised February 21, 2023; accepted February 26, 2023; published online March 27, 2023

Previously, we proposed an ultrasonic measurement method of arterial wall elasticity for the early detection of arteriosclerosis. Since vascular wall elasticity depends on blood pressure, in this study, the elasticity and viscosity were estimated using the hysteresis loop determined between the incremental strain in the wall and internal pressure by altering the internal pressure in the phantom and in vivo experiments. Consequently, both the estimated elasticity and viscosity increased with the internal pressure. Moreover, the slope of each hysteresis loop was larger than that of the approximated curve for the lowest blood pressures of the hysteresis loops with different internal pressures, as the blood pressure changed in the order of several hertz within a single heartbeat. Hence, we conclude that measuring both the blood pressure and the elastic and viscous moduli would be beneficial in comprehensively investigating more vessel wall properties that change with the progression of arteriosclerosis.

1. Introduction

Cardiovascular and cerebrovascular diseases are the leading causes of death worldwide.[1)] Early diagnosis of arteriosclerosis, the main cause of these diseases, is necessary to prevent them. In the early stages of arteriosclerosis, the cholesterol content in the aorta severely affects the elastic properties of the arterial wall,[2)] and the early detection of arteriosclerosis can be expected by evaluating the elasticity of the arterial wall.

The pulse wave velocity (PWV) measurement,[3–5)] flow-mediated dilatation (FMD) test[6,7)] and arterial-wall thickness-change measurement[8,9)] can be adopted to noninvasively and repeatedly evaluate the elastic properties of the arterial wall. The PWV measurement can solely evaluate the average elastic properties of the entire measurement area. Accurate evaluation with the FMD test is difficult because the distance resolution via ultrasonic measurement is insufficient. In contrast, ultrasound can be used to evaluate tissue properties in vivo.[10,11)] The method used to measure the wall thickness change for each ultrasonic beam can estimate the local elasticity of the arterial wall.[12–16)]

Kanai et al. developed the phased-tracking method and measured minute displacement in heart and blood vessels in the order of tens of microns, which were not measured with the spatial resolution of conventional ultrasound systems.[17,18)] The elastic modulus of the vessel wall was estimated by measuring the local thickness change during a heartbeat and the pulse pressure using a sphygmomanometer. Since blood vessels are viscoelastic media, the relationship between the blood pressure and strain draws a hysteresis loop. Assuming a viscoelastic model, it is possible to qualitatively determine not only the elasticity, but also the viscosity of the vessel wall from the hysteresis loop between the inner diameter change and blood pressure. Furthermore, by fitting the hysteresis loop to a viscoelastic model, such as the Voigt model, the elastic and viscous moduli can be quantitatively determined. To obtain a hysteresis loop, the blood pressure waveform and strain waveform should be measured simultaneously. In the previous study, since the blood pressure and thickness change could not be measured simultaneously at the same position using the normal ultrasound probe, only the elastic modulus was estimated, although the blood vessel is a viscoelastic medium. Therefore, Arakawa et al. have developed an ultrasound probe with a center frequency of 7.5 MHz that can measure blood pressure waveform with a central element.[19–21)] Since the radial artery is close to the skin and just above the radius, the pressure waveform can be obtained by pressing the probe, including the piezoelectric element, against the radial artery through the skin. The thickness change in the radial artery cannot be measured because of the insufficient distance resolution. However, using this probe, changes in the inner diameter and blood pressure were simultaneously measured at the same position.

Hypertension is one of the factors of arteriosclerosis.[22,23)] In hypertension, vascular endothelial cells are damaged and the basis for arteriosclerosis is formed.[24)] The elasticity of the vascular wall is known to depend on blood pressure.[25–27)] The vascular wall comprises elastin, collagen, and smooth muscle. The elastic properties are dominated by soft elastin and stiff collagen at low and high blood pressures, respectively.[28)] The relationship between the internal pressure $p(t)$ and inner diameter $d_i(t)$ is expressed using the reference pressure A_{ref} and inner diameter d_{iref} at the reference pressure A_{ref}, as $p(t) = A_{ref} \cdot \exp(\beta \cdot (d_i(t)/d_{iref} - 1))$, where β is the stiffness parameter.[29)] The stiffness parameter β is an index of elastic properties independent of blood pressure.[25,30)] However, it is a dimensionless parameter that reflects the apparent elastic property of the arterial wall. If the blood pressure dependence on the viscoelasticity of blood vessels could be measured in vivo, the steady-state load exerted by blood pressure on blood vessels can be determined, and this may facilitate the establishment of diagnostic guidelines for arteriosclerosis by measuring the viscoelastic properties. Moreover, because the vascular wall is a viscoelastic medium, the estimated viscoelastic properties may differ under static and dynamic conditions, such as in vivo, where the vascular wall is beating.

In the present study, by comparing the blood pressure dependence of the viscoelastic properties of the vascular wall

under dynamic conditions, we demonstrated the importance of measuring them in vivo. As a preliminary study, we measured the hysteresis loops between the internal pressure and vascular inner diameter with varying minimal internal pressure and then investigated the internal pressure dependence of the vascular wall's viscoelasticity. First, we constructed a phantom experimental system with an adjustable internal pressure. The internal pressure of the phantom was varied while the pulse pressure was kept consistent, and the hysteresis loops between the inner diameter change and internal pressure were investigated.[31] Moreover, the elasticity and viscosity were estimated. In in vivo experiments, the diastolic blood pressure was varied in the radial artery by altering the height of the radial artery from the heart, the hysteresis loops between the blood pressure and inner diameter were obtained, and the viscoelasticity was estimated using the developed probes.[19–21]

2. Experimental method

2.1. Measurement of viscoelasticity using change in the inner diameter

The elasticity and viscosity of the wall were estimated by simultaneously measuring the inner diameter change $\Delta d_i(t)$ of the phantom or blood vessel and internal pressure (blood pressure) $p(t)$. The inner diameter change $\Delta d_i(t)$ occurring with pulsation was calculated by integrating the minute velocity waveforms at the inner sides of the anterior and posterior walls.[32] The minute velocity waveform was obtained using the phased-tracking method.[17] It was assumed that the phantom or vessel wall is isotropic, elastically incompressible, uniform in wall thickness, and expansion and contraction do not occur in the longitudinal direction.[33–35] The relationship between the strain $\Delta d_i(t)/d_{i0}$ due to the inner diameter change $\Delta d_i(t)$ and incremental internal pressure $\Delta p(t)$ can be expressed by Eq. (1), assuming the Voigt model, and considering the viscous term:

$$E\frac{\Delta d_i(t)}{d_{i0}} + \eta\frac{\partial}{\partial t}\frac{\Delta d_i(t)}{d_{i0}} = \frac{3}{8}\frac{(h_0+d_{i0})(2h_0+d_{i0})}{h_0 d_{i0}}\Delta p(t) = \Delta\sigma(t), \tag{1}$$

where d_{i0} and h_0 denote the inner diameter and thickness, respectively, of the phantom or vessel at the minimum internal pressure; E and η are the elasticity and viscosity, respectively, of the phantom or arterial wall. The right-hand side of Eq. (1) shows the incremental stress $\Delta\sigma(t)$. In the derivation of Eq. (1), it is assumed that the inner diameter change $\Delta d_i(t)$ and outer diameter change $\Delta d_o(t)$ are sufficiently smaller than the inner diameter d_{i0} and outer diameter d_{o0} at the minimum internal pressure, respectively ($|\Delta d_i(t)| \ll d_{i0}$, $|\Delta d_o(t)| \ll d_{o0}$). The inner diameter d_{i0} and thickness h_0 of the phantom at the minimum internal pressure were obtained by the time-of-flight method using ultrasound.[36] The elasticity E and viscosity η were estimated to minimize the squared error between the measured incremental internal pressure $\Delta p(t)$ and model $\widehat{\Delta p}(t)$, as expressed in Eqs. (2) and (3), respectively:

$$E = \frac{\overline{\sigma(t)\left(\frac{\Delta d_i(t)}{d_{i0}}\right)}\cdot\overline{\left(\frac{\partial}{\partial t}\frac{\Delta d_i(t)}{d_{i0}}\right)^2} - \overline{\sigma(t)\left(\frac{\partial}{\partial t}\frac{\Delta d_i(t)}{d_{i0}}\right)}\cdot\overline{\left(\frac{\Delta d_i(t)}{d_{i0}}\right)\left(\frac{\partial}{\partial t}\frac{\Delta d_i(t)}{d_{i0}}\right)}}{\overline{\left(\frac{\Delta d_i(t)}{d_{i0}}\right)^2}\cdot\overline{\left(\frac{\partial}{\partial t}\frac{\Delta d_i(t)}{d_{i0}}\right)^2} - \left\{\overline{\left(\frac{\Delta d_i(t)}{d_{i0}}\right)\left(\frac{\partial}{\partial t}\frac{\Delta d_i(t)}{d_{i0}}\right)}\right\}^2}, \tag{2}$$

$$\eta = \frac{\overline{\sigma(t)\left(\frac{\partial}{\partial t}\frac{\Delta d_i(t)}{d_{i0}}\right)}\cdot\overline{\left(\frac{\Delta d_i(t)}{d_{i0}}\right)^2} - \overline{\sigma(t)\left(\frac{\Delta d_i(t)}{d_{i0}}\right)}\cdot\overline{\left(\frac{\Delta d_i(t)}{d_{i0}}\right)\left(\frac{\partial}{\partial t}\frac{\Delta d_i(t)}{d_{i0}}\right)}}{\overline{\left(\frac{\Delta d_i(t)}{d_{i0}}\right)^2}\cdot\overline{\left(\frac{\partial}{\partial t}\frac{\Delta d_i(t)}{d_{i0}}\right)^2} - \left\{\overline{\left(\frac{\Delta d_i(t)}{d_{i0}}\right)\left(\frac{\partial}{\partial t}\frac{\Delta d_i(t)}{d_{i0}}\right)}\right\}^2}, \tag{3}$$

where $\bar{\cdot}$ represents the average operation during one beat.

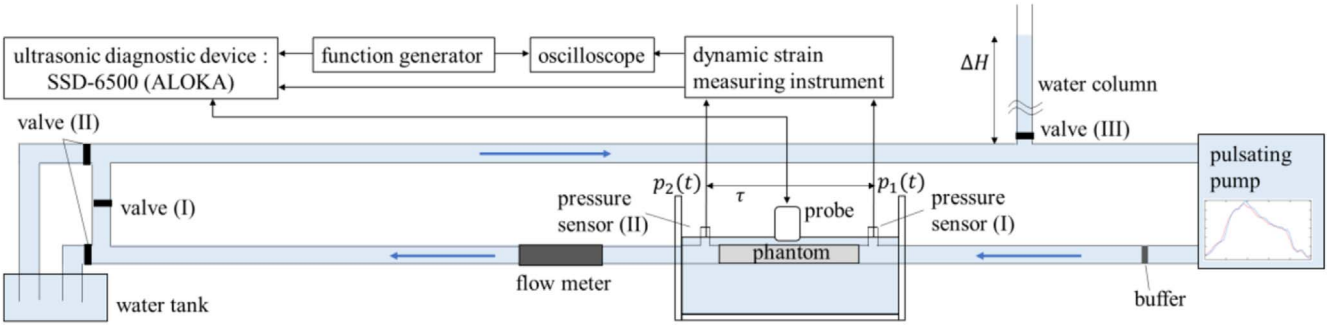

Fig. 1. (Color online) Schematic diagram of the phantom experimental system.

2.2. Phantom experiments

Figure 1 shows a schematic diagram of the experimental phantom system. A pulsatile pump (EC-8, Fuyo, Japan) was utilized to circulate water in a closed circulation path, not passing the tank, to simulate in vivo blood circulation (valve I: open, valve II: closed). Moreover, the water column applied hydrostatic pressure in the pathway (valve III: open) to achieve hydrostatic pressure as high as the in vivo condition, regardless of the flow rate from the pump.

In the ultrasound measurement, a linear probe with a center frequency of 7.5 MHz was connected to an ultrasonic diagnostic device (SSD-6500, Aloka, Japan). The sampling frequency, beam spacing and frame rate were 40 MHz, 150 μm and 286 Hz, respectively. A silicone rubber tube with an Asker C hardness of 10°, outer diameter of 9 mm, inner diameter of 7 mm and wall thickness of 1 mm (all nominal values) with graphite added as a scatterer was adopted as a phantom to mimic the carotid artery. The pulsation rate was set at 70 times min^{-1}.

In the phantom experiment, the probe developed by our group was not used because the internal pressure was measured directly using pressure sensors. The internal pressures $p_1(t)$ and $p_2(t)$ were measured by pressure sensors (I) and (II) (PS-1KC, Kyowa, Japan) positioned upstream and downstream of the phantom, respectively. The delay time τ between the two pressure waveforms $p_1(t)$ and $p_2(t)$ was determined using the cross-correlation function. The inner diameter of the phantom, $d_i(t)$, was measured using ultrasound at equidistant positions from the two pressure sensors. The pressure waveforms $p_1(t)$ and $p_2(t)$ were shifted by $\tau/2$ to compensate for the delay time due to the different measurement positions between the inner diameter waveform $d_i(t)$ and internal pressure waveforms $p_1(t)$ or $p_2(t)$. To obtain the hysteresis loops between the internal diameter $d_i(t)$ and internal pressure $p(t)$ and estimate elasticity E and viscosity η, $p_1(t - \tau/2)$ measured upstream the phantom was adopted.

To simulate in vivo blood pressure conditions, the steady-state water column height ΔH was set at 130 cm so that the maximum and minimum water pressures were 120 mmHg (160 cmH_2O) and 75 mmHg (100 cmH_2O), respectively. For comparison, the height ΔH of the water column was set at 30 (the maximum and minimum water pressures were 45 and 0 mmHg, respectively), 60 (70 and 20 mmHg) and 100 cm (90 and 45 mmHg). The hysteresis loops were measured by varying the minimum internal pressure from 0 to 75 mmHg. Furthermore, the changes in the slope and viscoelasticity are discussed. At each water column height ΔH, the hysteresis loops between the inner diameter waveform $d_i(t)$ and internal pressure waveform $p(t)$ were measured for four beats to estimate elasticity E and viscosity η. The instantaneous flow rate $q(t)$, measured with a flowmeter (FD-XS20, Keyence, Japan), was used to estimate the flow rate per pulsation Q, and the flow volume from the pump was set so that the water flow rate Q was approximately 600 ml min^{-1}, corresponding to the blood flow rate in the carotid artery.

2.3. In vivo experiments

Figure 2(a) shows a schematic diagram of the in vivo experimental system. The subject was a healthy female in her twenties, and her inner diameter $d_i(t)$ and blood pressure waveform $p(t)$ in the radial artery of her left hand were measured. In in vivo experiments, pressure sensors cannot be used to measure blood pressure waveforms. Thus, the blood pressure waveform can be measured using the linear probe developed by our research group.[19–21] The linear probe was connected to an ultrasonic diagnostic device (Prosound F75; Aloka, Japan). The center frequency, sampling frequency and frame rate were set at 7.5 MHz, 40 MHz and 252 Hz, respectively.

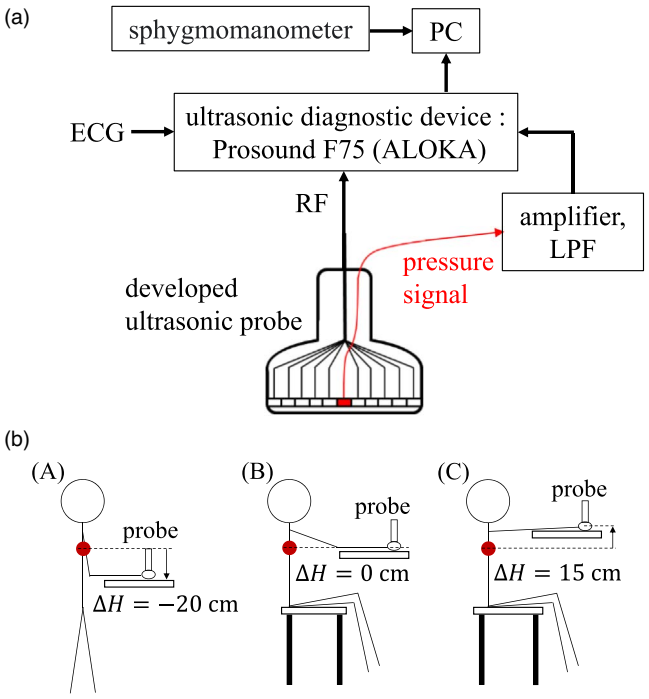

Fig. 2. (Color online) Schematic diagram of the in vivo experimental system. (a) Block diagram and (b) arm position during the experiment.

While viewing the B-mode short-axis image of the radial artery, the measurement position was set so that the center of the ultrasound probe was just above the radial artery, and the probe was pressed against the radial artery with an appropriate force to measure the blood pressure waveform. The output from the piezoelectric element at the center of the ultrasound probe passed through an amplifier with an amplification factor of 40 dB and a low-pass filter with a cut-off frequency of 30 Hz, and the blood pressure waveform was obtained by integrating the output waveform.

To acquire the internal pressure $p(t)$ and inner diameter $d_i(t)$ in the radial artery under different blood pressure conditions, the values were measured in three different situations, as shown in Fig. 2(b): (A) when the radial artery was 20 cm lower than the heart ($\Delta H = -20$ cm), (B) at the same height as the heart ($\Delta H = 0$ cm), and (C) 15 cm higher than the heart ($\Delta H = 15$ cm). At each arm position, the hysteresis loops between the inner diameter waveform $d_i(t)$ and blood pressure waveform $p(t)$ were measured for two heartbeats to estimate elasticity E and viscosity η. The radial-artery wall thickness could not be measured by the probe with a center frequency of 7.5 MHz due to the lack of distance resolution. Hence, a probe with a center frequency of 40 MHz was connected to an ultrasonic diagnostic device (UD-8000, Tomey, Japan) to measure the wall thickness h_0 of the subject's radial artery beforehand.

As the blood pressure waveform measured with our probe was output as a voltage, calibration was required to obtain the

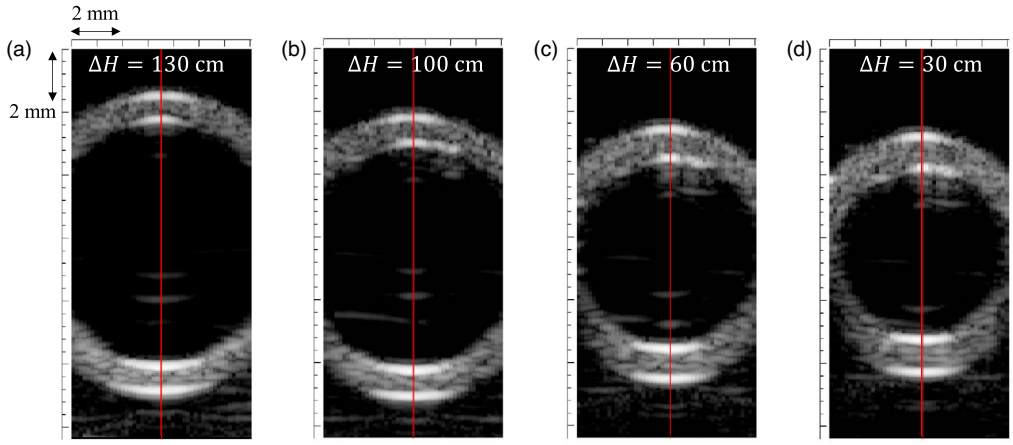

Fig. 3. (Color online) B-mode images of the phantom. Red line depicts the analyzed beam. (a) 130 cmH_2O, (b) 100 cmH_2O, (c) 60 cmH_2O, (d) 30 cmH_2O and (e) 0 cmH_2O.

absolute value of the blood pressure. Diastolic and systolic blood pressures were measured at three different heights at the same positions as the ultrasound measurement shown in Fig. 2(b), using a wrist-measurable sphygmomanometer (WS-20J, Japan Precision Instruments, Japan) after the ultrasound measurement, and the blood pressure waveforms were calibrated.[19,20] These measurements were approved by the Ethics Committee of the Graduate School of Engineering Tohoku University, and all the participants provided consent before participating in the present study.

3. Results

3.1. Phantom experiments

By setting the output of the pulsating pump, the flow rate Q of water per pulsation was 611 ± 10 ml min^{-1}, thereby simulating the blood flow condition in the carotid artery. Figure 3 shows B-mode images at minimum pressures (a) when the height of the water column ΔH was 130 cm, and in vivo blood pressure conditions were simulated (minimum pressure at a beat: 70 mmHg), (b) 100 cm (45 mmHg), (c) 60 cm (20 mmHg) and (d) 30 cm (0 mmHg). The inner diameter $d_i(t)$ was obtained by analyzing the beam depicted by the red line. The minimum inner diameters d_{i0} at the minimum internal pressure were (a) 9.76 mm, (b) 8.98 mm, (c) 7.51 mm and (d) 6.81 mm. The minimum posterior wall thicknesses h_0 at the minimum internal pressure were (a) 0.67 mm, (b) 0.72 mm, (c) 0.84 mm and (d) 0.90 mm. The higher the water column and internal pressure $p(t)$, the larger the inner diameter $d_i(t)$ and the thinner the wall thickness $h(t)$.

Figure 4 shows (a) the internal pressure $p(t)$ for four circulation cycles when the height ΔH of the water column was 130 cm (minimum pressure at a beat: 70 mmHg) (in vivo condition), 100 cm (45 mmHg), 60 cm (20 mmHg) and 30 cm (0 mmHg), (b) the incremental strain $\Delta d_i(t)/d_{i0}$ of the inner diameter change $\Delta d_i(t)$, and (c) the hysteresis loops between the internal pressure $p(t)$ and inner diameter $d_i(t)$. Figure 4(a) demonstrates that the maximum and minimum pressures increased as the height ΔH of the water column was raised. Figure 4(b) demonstrates that the maximum strain increased from the height of the water column ΔH = 30 cm (blue) to 60 cm (green) and decreased from 60 cm (green) to 130 cm (red). Figure 4(c) demonstrates that the slope of the hysteresis loop increased as the height ΔH of the water column was increased. The hysteresis loops at the height of the water column ΔH = 130 cm (red) and 100 cm (yellow) have a larger slope at higher pressures, thus indicating a nonlinear relationship between the pressure $p(t)$ and inner diameter $d_i(t)$. The relationships between the internal pressure $p(t)$ and inner diameter $d_i(t)$ measured at different heights ΔH of the water column were not plotted on a single curve.

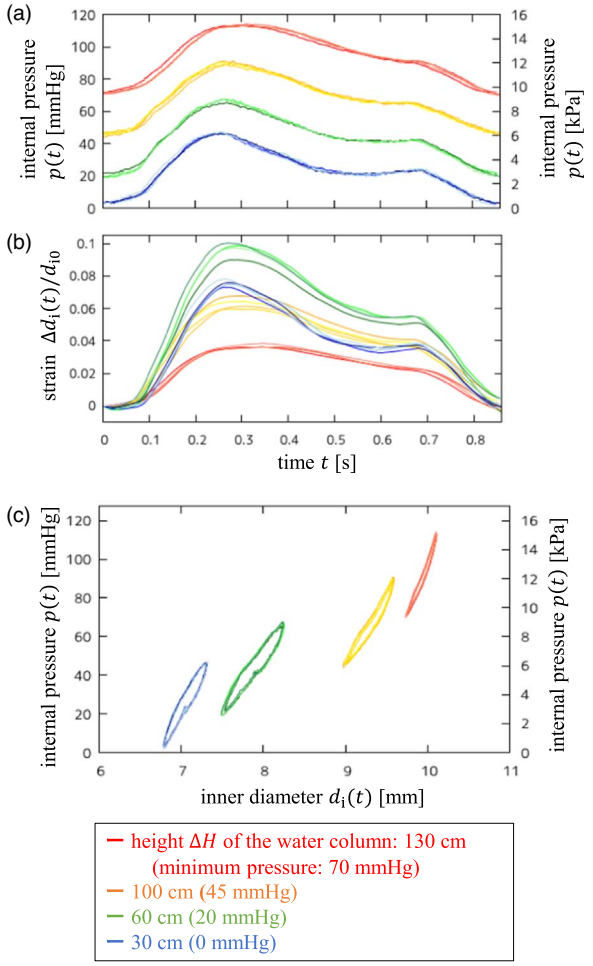

Fig. 4. (Color online) Results of the phantom obtained for four circulation cycles at each internal pressure: (a) internal pressure $p(t)$, (b) incremental strain of the thickness change, $\Delta h(t)/h_0$, and (c) hysteresis loops between the internal pressure $p(t)$ and inner diameter $d_i(t)$.

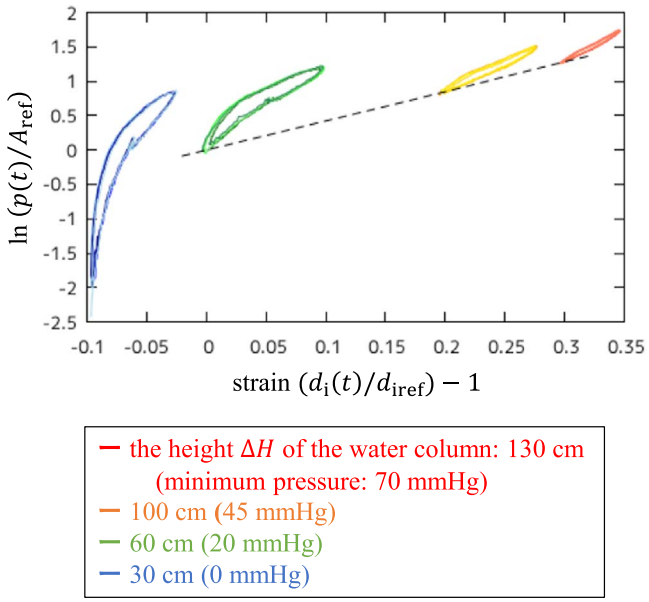

Fig. 5. (Color online) Results of the hysteresis loops for the phantom between the natural logarithms of $p(t)/A_{\mathrm{ref}}$, $\ln(p(t)/A_{\mathrm{ref}})$, and incremental strain of the inner diameter, $\Delta d_{\mathrm{i}}(t)/d_{\mathrm{iref}}$, for four circulation cycles at each internal pressure. Dashed line indicates the approximated straight line obtained for the pressures at the lowest pressure in the hysteresis loops when the heights of the water column ΔH were 130 (minimum pressure at a beat: 70 mmHg), 100 (45 mmHg) and 60 cm (20 mmHg).

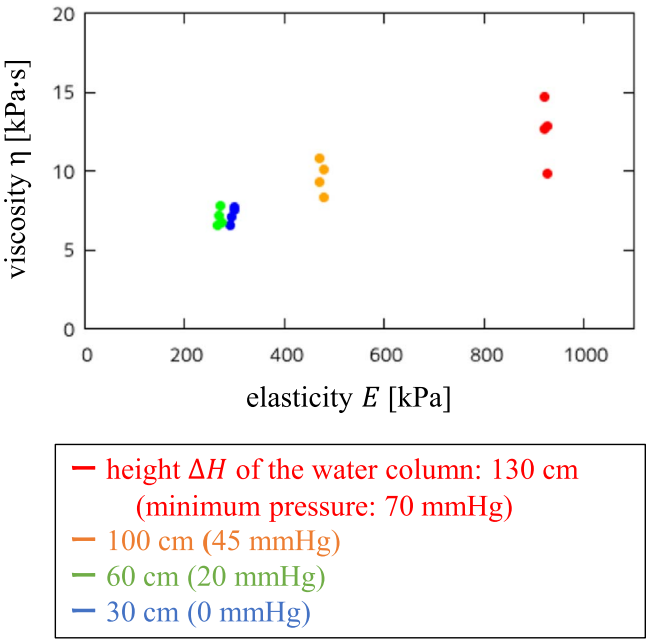

Fig. 6. (Color online) Elastic and viscous modulus values of the phantom estimated for four beats at each internal pressure.

The natural logarithm of the internal pressure $p(t)$ is calculated because the relationship between the internal pressure $p(t)$ and inner diameter $d_{\mathrm{i}}(t)$ is usually expressed as $p(t) = A_{\mathrm{ref}} \cdot \exp(\beta \cdot (d_{\mathrm{i}}(t)/d_{\mathrm{iref}} - 1))$, considering the nonlinearity of elasticity.[29] Here, A_{ref}, d_{iref} and β are the reference pressure, inner diameter at the reference pressure A_{ref} and stiffness parameter, respectively.

Figure 5 shows the hysteresis loops determined between the natural logarithms of $p(t)/A_{\mathrm{ref}}$, $\ln(p(t)/A_{\mathrm{ref}})$, and the strain in the inner diameter change $\Delta d_{\mathrm{i}}(t)/d_{\mathrm{iref}}$ in the phantom experiment. A_{ref} is the minimum internal pressure when the height ΔH of the water column is 60 cm. The dashed line in Fig. 5 indicates the approximated straight line obtained for the pressures at the lowest pressure in the hysteresis loops when the height of the water column ΔH is 130 (minimum pressure at beat: 70 mmHg), 100 (45 mmHg) and 60 cm (20 mmHg). Considering the hysteresis loop at each internal pressure, the mean values of the four beats with the lowest internal pressure and inner diameter at each time point were calculated. Using these values, an approximated straight line was obtained using the least squares method. The slope of the relationship between the natural logarithm of $p(t)/A_{\mathrm{ref}}$, $\ln(p(t)/A_{\mathrm{ref}})$, and the strain in the inner diameter change, $\Delta d_{\mathrm{i}}(t)/d_{\mathrm{i0}}$, is a straight line in the internal pressure range of 60–160 mmHg.[25] The internal pressures at the lowest pressures in the hysteresis loops were approximately on a straight line in this range.

Next, we focused on the estimated elasticity E and viscosity η for four consecutive circulation cycles using Eqs. (2) and (3); they are approximately the same when the height ΔH of the water column is 30 (blue) or 60 cm (green). However, these factors increase as the internal pressure increases for $\Delta H = 100$ (yellow) and 130 cm (red), as shown in Fig. 6. Hence, when the height ΔH of the water column was greater than $\Delta H = 60$ cm (20 mmHg), both elasticity E and viscosity η of the phantom depended on the internal pressure $p(t)$.

3.2. In vivo experiments

The wall thickness of the radial artery was measured as $h_0 = 0.20$ mm beforehand. Figure 7 shows the B-mode images of the radial artery at the minimum blood pressure when the radial artery was (a) 20 cm lower than the heart ($\Delta H = -20$ cm), (b) at the same height as the heart ($\Delta H = 0$ cm), and (c) 15 cm higher than the heart ($\Delta H = 15$ cm). The inner diameters (short diameters) d_{i0} were (a) 1.68 mm, (b) 1.60 mm and (c) 1.55 mm.

Figure 8 shows the hysteresis loops between the internal pressure $p(t)$ and inner diameter $d_{\mathrm{i}}(t)$ for two heartbeats when the radial artery was (A) 20 cm lower than the heart ($\Delta H = -20$ cm), (B) at the same height as the heart ($\Delta H = 0$ cm), and (C) 15 cm higher than the heart ($\Delta H = 15$ cm). Similar to the phantom experimental results, the slope of the hysteresis loop increased with increasing blood pressure, and the hysteresis loops at the three different blood pressures were not plotted on a single curve. The dashed line in Fig. 8 indicates the exponential function representing the relationship between the minimum blood pressure and inner diameter at that time for each hysteresis loop. The mean values of the two heartbeats with the lowest internal pressure and inner diameter at each time point were calculated in the hysteresis loop at each internal pressure. Using these values, an approximate curve was obtained using the least squares method.

Figure 9 shows the hysteresis loops between the natural logarithm of $p(t)/A_{\mathrm{ref}}$, $\ln(p(t)/A_{\mathrm{ref}})$, and the strain in the inner diameter change, $\Delta d_{\mathrm{i}}(t)/d_{\mathrm{iref}}$, from the in vivo experiment and the approximated straight line for the lowest pressure of the hysteresis loops (dashed line). A_{ref} is the minimum internal pressure when the radial artery was (C) 15 cm above the heart ($\Delta H = 15$ cm). Similar to the phantom experimental results, the blood pressure at the

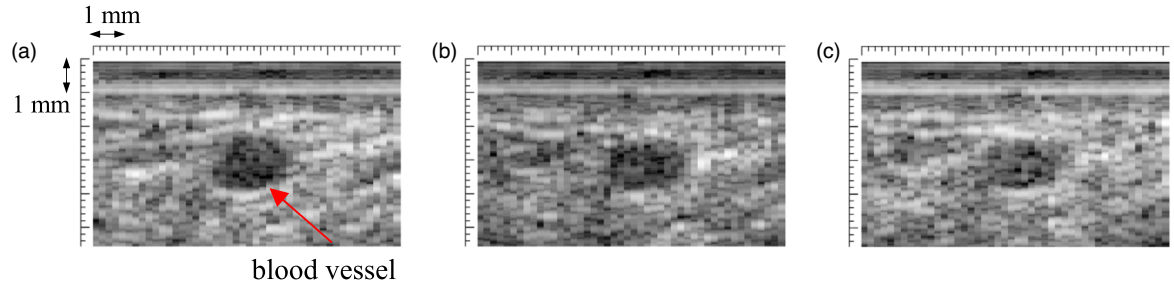

Fig. 7. (Color online) B-mode images of the radial artery: (a) arm position (A), (b) arm position (B), and (c) arm position (C) in Fig. 2.

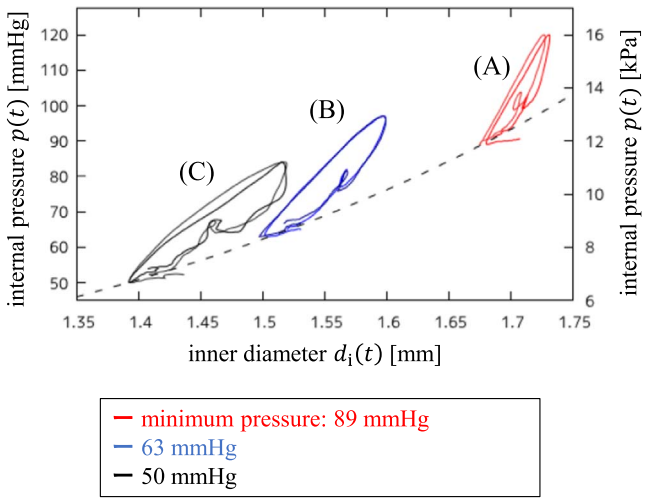

Fig. 8. (Color online) Results of the hysteresis loops for the radial artery between the internal pressure $p(t)$ and inner diameter $d_i(t)$ for two circulation cycles at each arm position. Dashed line indicates the exponential function representing the relationship between the lowest blood pressure and inner diameter at that time for each hysteresis loop.

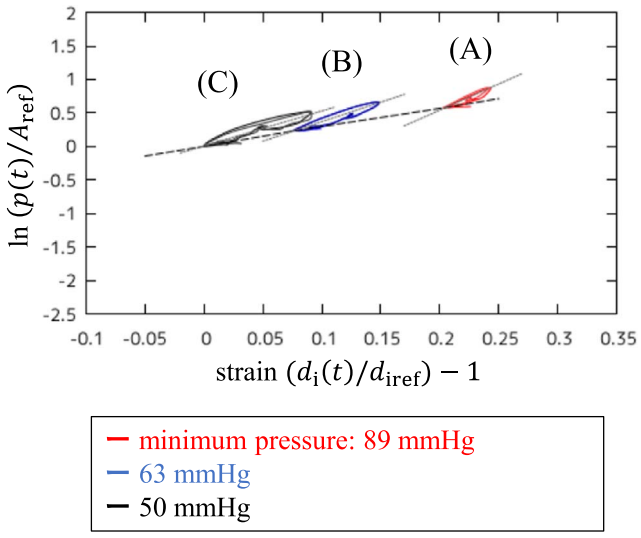

Fig. 9. (Color online) Results of the hysteresis loops for the radial artery between the natural logarithms of $p(t)/A_{ref}$, $\ln(p(t)/A_{ref})$, and incremental strain of the inner diameter, $\Delta d_i(t)/d_{iref}$, for two circulation cycles at each arm position. Dashed line indicates the approximated straight line for the blood pressures at the lowest pressure of the hysteresis loops. Gray line on each hysteresis loop shows the slope of each hysteresis loop.

minimum blood pressure in each hysteresis loop was approximated as a straight line.

Elasticity E and viscosity η estimated for the two heartbeats using Eqs. (2) and (3), are shown in Fig. 10. When the

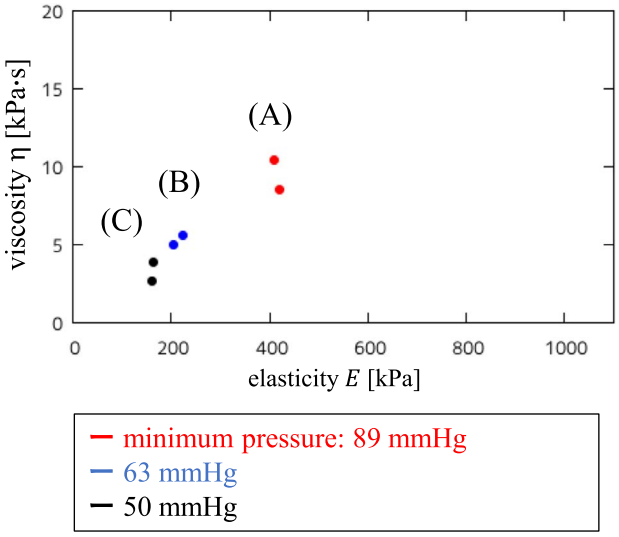

Fig. 10. (Color online) Elastic and viscous modulus values of the radial artery estimated for two heartbeats at each arm position.

radial artery was lower than the heart (high blood pressure) (red), elasticity E and viscosity η were estimated to be higher than when the radial artery was at the same height as the heart (blue), and when the radial artery was higher than the heart (low blood pressure) (black), they were estimated to be lower. Similar to the phantom experimental results, elasticity E and viscosity η depended on the internal pressure, i.e. the blood pressure.

4. Discussion

In our previous study, we confirmed that the strain of the outer diameter change and elasticity E could be measured ultrasonically with the same accuracy as those obtained via laser.[36] In the present study, elasticity E was estimated from the change in the inner diameter. The resulting E agreed with that estimated from the change in the outer diameter within 4%. Therefore, the appropriate elasticity E can be estimated from the change in the inner diameter. However, the validity of viscosity η needs to be verified in future studies.

In both the phantom and in vivo experiments, as the internal pressure $p(t)$ increased, the estimated elasticity E increased, as shown in Figs. 6 and 10. As the internal pressure increased, the strain $\Delta d_i(t)/d_{i0}$ became smaller, as shown in Fig. 4(b), and the phantom and blood vessels elongate significantly and are less deformed.

In the phantom experiment, as shown in Fig. 4(c), when the height ΔH of the water column is 60 cm, the slope of the hysteresis loop is smaller than that when ΔH is 30 cm;

however, both estimated elasticities E are approximately the same. Specifically, the slope in Fig. 4(c) does not represent elasticity E. Elasticity E is related to the slope of the incremental stress $\Delta\sigma(t)$ concerning strain $\Delta d_i(t)/d_{i0}$, which was nearly the same at 0 and 30 cm height ΔH of the water column.

Next, we discuss viscosity η. In the phantom experiment, as the internal pressure increases, the area of the hysteresis loop decreases, as shown in Fig. 4(c), whereas viscosity η increases, as shown in Fig. 6. This is because the area of the hysteresis loop is determined not by viscosity but by the ratio of viscosity to elasticity, η/E. When the height ΔH of the water column was 130 cm, elasticity E and viscosity η were approximately three and two times higher, respectively, than those at 30 cm. This indicates that the area of the hysteresis loop with $\Delta H = 130$ cm was smaller than that with $\Delta H = 30$ cm. In contrast, the areas of the hysteresis loops were approximately the same when the internal pressure was varied, and elasticity E and viscosity η changed at a constant rate in the in vivo experiment.

In the phantom and in vivo experiments, the variance in viscosity η was larger than that in elasticity E, as shown in Figs. 6 and 10. Since the differentiation of strain results in a larger error, the difference in viscosity η is larger than that in elasticity E. Furthermore, in the phantom experiments, the variance in viscosity η increases as the internal pressure $p(t)$ increases. The variance in viscosity η increases as the amplitude of the differential waveform $\partial(\Delta d_i(t)/d_{i0})/\partial t$ of the strain decreases. The greater the internal pressure $p(t)$, the greater the elasticity E and the smaller the strain $\Delta d_i(t)/d_{i0}$. Therefore, the derivative $\partial(\Delta d_i(t)/d_{i0})/\partial t$ of strain is also smaller, resulting in greater viscosity variance.

Next, we compared the viscoelasticity of the phantom in Fig. 6 and in vivo experimental results in Fig. 10. The estimated E and η were of the same order in the phantom and in vivo experiments. This confirms that the E and η of blood vessels depend on the blood pressure in the normal in vivo blood pressure range.

The hysteresis loops in Fig. 9 and those formed when the heights ΔH of the water column were 130 cm (diastolic pressure at beat: 70 mmHg), 100 cm (45 mmHg) and 60 cm (20 mmHg) in Fig. 5 were not represented in a single straight line. The slope of each hysteresis loop was larger than that of the approximated straight line for the lowest blood pressures. When the relationship between the internal pressure $p(t)$ and inner diameter $d_i(t)$ is expressed by an exponential function,[25] each hysteresis loop can be expressed on a straight line. In the present study, the frequency dependence was not considered in the viscoelasticity estimation. However, in the Voigt model, the complex elastic modulus E^* is represented as $E + j\omega\eta$, and the imaginary part of the complex elastic modulus E^* increases as the frequency increases. The reason for the larger slope of the hysteresis loops is that the absolute value of the complex elastic modulus E^* increased due to blood pressure changes of several hertz within a single heartbeat. As shown in Fig. 9, the slope of the hysteresis loop increased as the internal pressure increased. Since the conventional stiffness parameter β is also measured under dynamic conditions, it is suggested that β may also depend on the internal pressure, although it has been reported that it does not depend on the internal pressure.[25]

5. Conclusion

In the present study, to investigate the blood pressure dependence of the viscoelastic properties of blood vessels, the hysteresis loops between the internal pressure $p(t)$ and inner diameter $d_i(t)$ were measured, and elasticity E and viscosity η were estimated by altering the internal pressure $p(t)$ in the phantom and in vivo experiments. The slopes of the hysteresis loops increased, and elasticity E and viscosity η were estimated to increase, as the internal pressure $p(t)$ increased. The internal pressure $p(t)$ is expressed as an exponential function of the inner diameter $\Delta d_i(t)$. In the in vivo experiments, the relationship between the minimum blood pressure and the inner diameter at the time of each hysteresis loop was expressed as an exponential function. However, the slope of each hysteresis loop was larger than that of the approximate curve (approximate straight line for the natural logarithm of blood pressure). This could be due to the effect of the blood pressure waveform frequency. Therefore, the frequency dependence of the viscoelastic properties of the vessel wall should be investigated in future. Simultaneous measurements of the internal pressure $p(t)$ and the incremental strain of the inner diameter $\Delta d_i(t)/d_{i0}$ by altering the internal pressure enabled us to measure the changes in elasticity E and viscosity η due to the blood pressure dependency. Hence, measuring the blood pressure, elasticity E and viscosity η would be beneficial in comprehensively investigating more detailed properties of the vessel wall that change with the progression of arteriosclerosis. In the future, we will apply this method to measure the blood pressure, elasticity E and viscosity η in patients with arteriosclerosis to demonstrate the usefulness of the early diagnosis of arteriosclerosis.

Acknowledgments

This work was supported in part by JSPS KAKENHI 21H03835.

1) K. J. Foreman et al., Lancet **392**, 2052 (2018).
2) T. I. Pynadath and D. P. Mukherjee, Atherosclerosis **26**, 311 (1977).
3) P. J. Brands, J. M. Willigers, L. A. F. Ledoux, R. S. Reneman, and A. P. G. Hoeks, Ultrasound Med. Biol. **24**, 1325 (1998).
4) Y. Nagai, J. L. Fleg, M. K. Kemper, T. M. Rywik, C. J. Earley, and E. J. Mette, Ultrasound Med. Biol. **25**, 181 (1999).
5) T. Pereira, C. Correia, and J. Cardoso, J. Med. Biol. Eng. **35**, 555 (2015).
6) M. Charakida, S. Masi, T. F. Lüscher, J. J. P. Kastelein, and J. E. Deanfield, Eur. Heart J. **31**, 2854 (2010).
7) J. Yeboah, A. R. Folsom, G. L. Burke, C. Johnson, J. F. Polak, W. Post, J. A. Lima, J. R. Crouse, and D. M. Herrington, Circulation **120**, 502 (2009).
8) A. P. G. Hoeks, C. Willekes, P. Boutouyrie, P. J. Brands, J. M. Willigers, and R. S. Reneman, Ultrasound Med. Biol. **23**, 1017 (1997).
9) S. Laurent, Hypertension **26**, 355 (1995).
10) T. Mizoguchi, K. Yoshida, J. Mamou, J. A. Ketterling, and T. Yamaguchi, Jpn. J. Appl. Phys. **59**, SKKE17 (2020).
11) R. Takagi and Y. Koseki, Jpn. J. Appl. Phys. **61**, SG1069 (2022).
12) J. Persson, L. Stavenow, J. Wikstrand, B. Israelsson, J. Formgren, and G. Berglund, Arterioscler. Thromb. **12**, 261 (1992).
13) H. Hasegawa, H. Kanai, Y. Koiwa, and P. Butler, Jpn. J. Appl. Phys. **42**, 3255 (2003).
14) H. Kanai, H. Hasegawa, M. Ichiki, F. Tezuka, and Y. Koiwa, Circulation **107**, 3018 (2003).
15) H. Hasegawa, H. Kanai, and Y. Koiwa, IEEE Trans. Ultrason. Ferroelectr. Freq. Control **51**, 93 (2004).

16) J. Inagaki, H. Hasegawa, H. Kanai, M. Ichiki, and F. Tezuka, Jpn. J. Appl. Phys. **44**, 4593 (2005).
17) H. Kanai, M. Sato, Y. Koiwa, and N. Chubachi, IEEE Trans. Ultrason. Ferroelectr. Freq. Control **43**, 791 (1996).
18) H. Hasegawa, H. Kanai, and Y. Koiwa, Jpn. J. Appl. Phys. **41**, 3563 (2002).
19) M. Arakawa, T. Saito, S. Mori, S. Ohba, K. Kobayashi, and H. Kanai, Sens. Actuators A **297**, 111487 (2019).
20) T. Saito, S. Mori, M. Arakawa, S. Ohba, K. Kobayashi, and H. Kanai, Jpn. J. Appl. Phys. **59**, SKKE04 (2020).
21) Y. Shoji, S. Mori, M. Arakawa, S. Ohba, K. Kobayashi, and H. Kanai, Jpn. J. Appl. Phys. **61**, SG1042 (2022).
22) W. Hollander, Am. J. Cardiol. **38**, 786 (1976).
23) N. Ishizaka, Y. Ishizaka, E. Toda, H. Hashimoto, R. Nagai, and M. Yamakado, Hypertens. Res. **28**, 27 (2005).
24) S. Taddei, A. Virdis, L. Ghiadoni, L. Sudano, and A. Salvetti, J. Cardiovasc. Pharmacol. **38**, S11 (2001).
25) K. Hayashi, H. Handa, S. Nagasawa, A. Okumura, and K. Moritake, J. Biomech. **13**, 175 (1980).
26) R. Busse, R. D. Bauer, A. Schabert, Y. Summa, P. Bumm, and E. Wetterer, Basic Res. Cardiol. **74**, 545 (1979).
27) R. L. Armentano, J. G. Barra, D. B. Santana, F. M. Pessana, S. Graf, D. Craiem, L. M. Brandani, H. P. Baglivo, and R. A. Sanchez, Hypertension **47**, 384 (2006).
28) J. E. Wagenseil and R. P. Mecham, J. Cardiovasc. Transl. Res. **5**, 264 (2012).
29) B. Spronck, A. P. Avolio, I. Tan, M. Butlin, K. D. Reesink, and T. Delhaas, J. Hypertens. **35**, 98 (2017).
30) K. Moritake, H. Handa, A. Okumura, K. Hayashi, and H. Niimi, Neurol. Med. Chir. **14pt1**, 47 (1974).
31) S. Suzuki, S. Mori, M. Arakawa, M. Iwai-Takano, and H. Kanai, Proc. Symp. Ultrason. Electr. **43**, 3Pa5 (2022).
32) H. Hasegawa, H. Kanai, N. Hoshimiya, and Y. Koiwa, J. Med. Ultrason. **31**, 81 (2004).
33) D. J. Patel, J. S. Janicki, R. N. Vaishnav, and J. T. Young, Circ. Res. **32**, 93 (1973).
34) H. Hasegawa and H. Kanai, Proc. 2007 IEEE Int. Ultrasonics Symp, 2007, p. 860.
35) Y. Miyachi, M. Arakawa, and H. Kanai, Jpn. J. Appl. Phys. **57**, 07LF08 (2018).
36) S. Akiyama, S. Mori, M. Arakawa, and H. Kanai, Jpn. J. Appl. Phys. **60**, SDDA07 (2021).